ACS OMEGA

http://pubs.acs.org/journal/acsodf

Article

Corrosion Behavior on 20# Pipeline Steel by Sulfate-Reducing Bacteria in Simulated NaCl Alkali/Surfactant/Polymer Produced Solution

Li Zhang, Xin Yu, He Sun, Yang Ge, Chao Wang, Limin Li, Jian Kang, Huijuan Qian, and Qinghe Gao*

Cite This: *ACS Omega* 2023, 8, 13955−13966

Read Online

ACCESS | Metrics & More | Article Recommendations

ABSTRACT: The corrosion behavior of sulfate-reducing bacteria (SRB) on 20# carbon steel in the NaCl alkali−surfactant−polymer (ASP) flooding system was studied by scanning electron microscopy, electrochemical measurement, X-ray photoelectron spectroscopy, and laser confocal microscopy. The results showed that the presence of SRB results in a large viscosity loss of the system. SRB can use hydrolyzed polyacrylamide (HPAM) as a nutrient to grow, and the number of SRB remained at a high level after 15 days. Weight loss and electrochemical tests indicated that SRB promoted corrosion of pipeline steel. The corrosion of carbon steel in the early stage of immersion was inhibited by the biofilm formed on the surface, and the thick biofilm in the later stage of immersion caused serious pitting corrosion. The localized corrosion caused by SRB was not inhibited by HPAM and sodium petroleum sulfonate (surfactant) adsorbed on the surface.

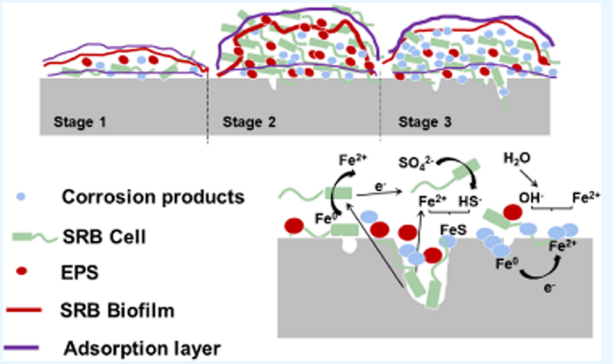

1. INTRODUCTION

The ever-increasing energy demand accelerates the deployment of oil and gas fields.[1] The effective life of existing oilfields with an efficiency of about 30−40% is coming to an end.[2] Currently, oil producers use the alkali−surfactant−polymer (ASP) technology to increase the reservoir pressure.[3] Nonetheless, the large amount of alkali would cause serious fouling to accumulate in the pipeline. To reduce fouling formation and lower the cost, researchers have found NaCl as an alternative for the partial replacement of alkali. The surfactant releases the interfacial tension between oil and water so that isolated oil can mobilize and the residual oil film can be removed. The addition of alkali reduces the adsorption retention loss of polymers and surfactants in the reservoir, whereas the polymer increases the viscosity of the solution meanwhile preventing the deactivation of the surfactant.[4] Polymers and surfactants interact with each other at the oil−water interface to form an adsorption layer with a high interfacial charge, which becomes thinner upon the addition of NaCl. In this way, it stabilizes the arrangement of surfactant molecules at the interface and helps maintain the long-term interfacial tension at a low level.[5] As a result, oil recovery is enhanced by the synergistic interaction of alkali, polymer, surfactant, and NaCl.

During oil production, water (produced water, formation water, or other water sources) is usually injected together with other oilfield chemicals.[6] As nutrients and oxidants are brought into the pipeline environment, microorganisms can easily reproduce in large numbers.[7] As the main backbone of production, carbon steel is used in almost all aspects of the oil and gas industry.[8] 20# low-carbon steel is widely found in oilfield transportation. It is prone to economic loss and personal injury due to the corrosion caused by microorganisms.[9,10] Microbial-influenced corrosion (MIC) in oilfield pipelines, which refers to the corrosion process that occurs with the participation of microbial life activities,[11] is mainly caused by sulfate-reducing bacteria (SRB).[12,13] MIC will generate potential impacts like pipeline failure, energy loss, and environmental hazards.[14,15] The first step of MIC involves the attachment of bacterial cells to the metal, forming a biofilm of extracellular polysaccharide substances (EPSs) on the metal surface.[10,16,17] EPSs include polymers such as polysaccharides, proteins, and nucleic acids.[17,18] The structure and uneven distribution of the biofilm forms an inconsistent surface environment, therefore promoting the corrosion of carbon steel.[19,20] The existence of the biocatalyst (biologically active ferments secreted by the SRB in the biofilm) accelerates the corrosion process because the reduction of cathodic sulfate

Received: January 19, 2023
Accepted: March 27, 2023
Published: April 6, 2023

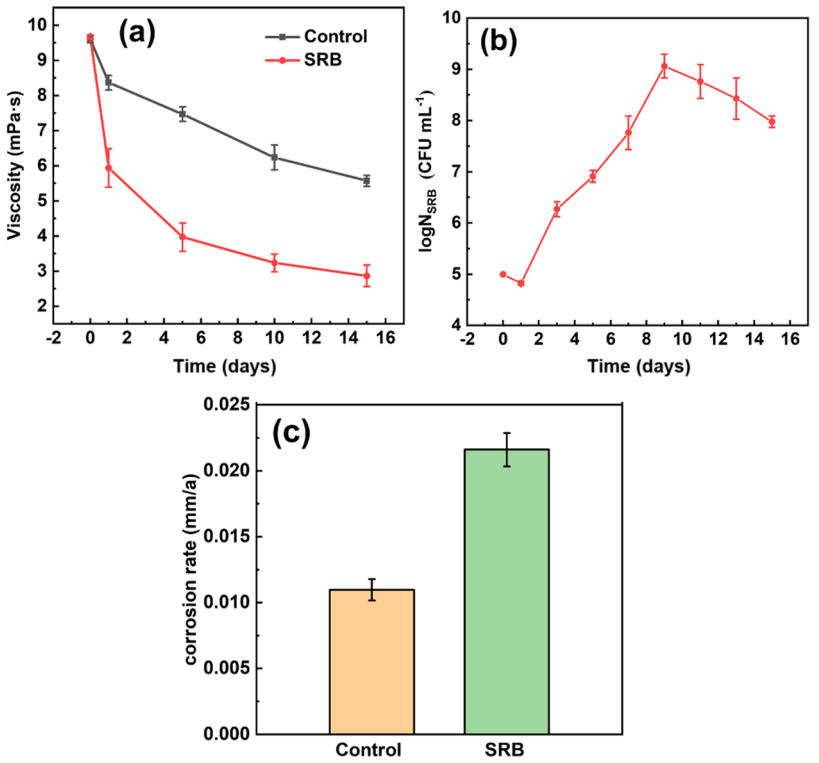

Figure 1. Viscosity of abiotic and inoculated ASP flooding recovery system (a); the growth curves of SRB conditions (b); and corrosion rates of metals under control and SRB medium (c).

directly consumes the electrons released by the dissolution of the anode metal material.[13] The corrosion product FeS comes from the metabolite H_2S of SRB, which will further enhance the corrosion of carbon steel by forming an effective cathode and anode.[21] Meanwhile hydrogen is produced by dissolving H_2S in water. Hydrogen penetration and crack corrosion of metals is caused by H_2.[22] The uneven diffusion of oxygen is caused by the uneven structure and distribution of microbial membranes on the metal surface. Consequently, the potential difference on the surface of the carbon steel ends up in serious pitting and crevice corrosion.

To date, researchers have studied the corrosion caused by SRB in oilfield pipeline steel.[23−25] However, most studies focus on conventional systems. As NaCl ASP flooding is a new enhanced oil recovery technology in recent years, there are a few studies on the corrosion of SRB in pipeline steel. Moreover, the existence of polymers in the system and the weak alkaline pH are bound to provide a better living environment for SRB and pose a great hidden danger to pipeline safety.[26] The purpose of this study is to better understand the corrosion behavior of 20# pipeline steel in the NaCl ASP flooding system under the action of SRB and provide a reference for on-site microbial corrosion protection.

2. RESULTS

2.1. System Environmental Parameters and Metal Corrosion. Figure 1a shows the variation of viscosity during the 15-day incubation with and without SRB in the produced water of the NaCl ASP flooding. The viscosity decreases distinctly in the first few days and then tends to stabilize in both control and SRB media. The viscosity of the SRB system decreased more than that of the control system. Hydrolyzed polyacrylamide (HPAM) was dissolved in water and dissociated into negatively charged macromolecules. The electrostatic repulsion among molecules and the anionic repulsion among different links on the same molecule led to the extension of molecules in solution and entanglement.[27,28] In the control medium, dissolved oxygen reacted with HPAM and caused the HPAM to degrade. The viscosity of the system decreases with HPAM degradation. In the SRB medium, HPAM was used as a nutrient for the growth of SRB, therefore it shows a higher decrease in viscosity than in the control medium.

The growth curve of the counts of SRB planktonic cells with time in the SRB medium is shown in Figure 1b. The planktonic cell count of viable SRB (N_{SRB}) decreased on the first day and then started to increase. This indicates that SRB in the system adapted to the new organic carbon source after a lagging phage and began to consume the polymer as a nutrient for growth. The N_{SRB} reaches the maximum on the 9th day, but then it started to decrease, which implies that SRB cells began to die.

As shown in Figure 1c, the corrosion rate of the metal under the control system is 0.0110 mm/a, and that in the SRB system is 0.0216 mm/a. The presence of SRB results in a greater weight loss of metal.

2.2. Analyses of Surface Morphology and Contact Angle. The surface morphology of 20# coupons after immersion in sterile and inoculated systems for 15 days was determined by scanning electron microscopy (SEM). As shown in Figure 2a, the surface of the coupon is covered by a thin corrosion product layer together with large and continuous corrosion particles after exposure to the control medium for 2 days. Scratches during pretreatment are observed at high magnification (Figure 2a$_1$). After 6 days of immersion, the surface of the coupon is covered with a thick corrosion product layer as well as minor corrosion particles

https://doi.org/10.1021/acsomega.3c00391
ACS Omega 2023, 8, 13955−13966

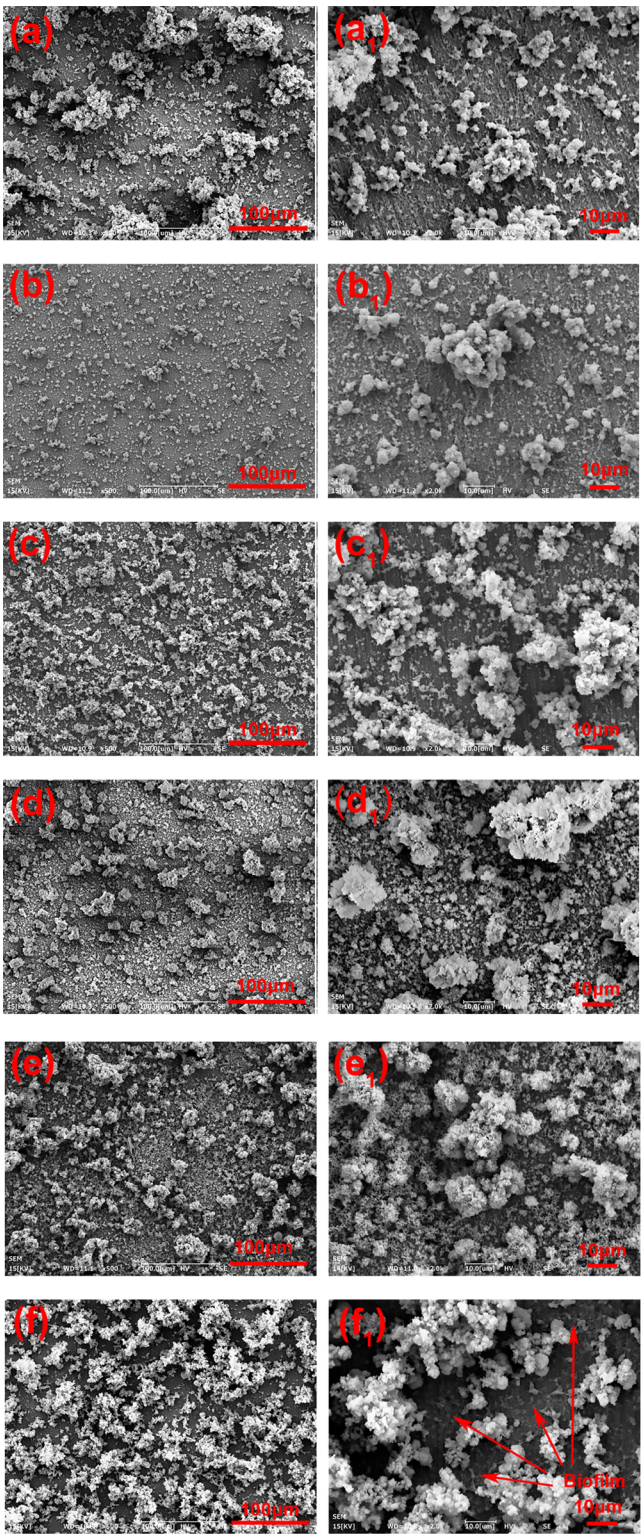

Figure 2. SEM images of corrosion products and microbial biofilm on the 20# coupon surface after 2, 6, and 15 days. Control (a; a_1, b; b_1, c; c_1); SRB (d; d_1, e; e_1, f; f_1).

($2b_1$). After immersion for 15 days, the coupon exhibited similar morphology with an increase in the number of corrosion particles. After immersion in the SRB medium for 2 days, a thicker corrosion product layer is observed on the surface of the coupon compared to that in the control medium. The coupon exhibited similar morphology after 6 days. The surface of the coupon is covered by scattered corrosion product particles after 15 days. SRB cells are observed to appear on the surface of the coupon and an extensive biofilm network was formed in the SRB-containing solution ($2f_1$).

The elemental compositions as well as the SEM images obtained after 15 days are shown in Table 1. There is a small amount of S element on the surface of the control medium, which was caused by the presence of SPS. The content of the S element in SRB-containing solution is higher than that in the control medium, which can be attributed to the typical corrosion product FeS in the presence of SRB.

Table 1. Energy-dispersive Spectrometry (EDS) Results of Corrosion Products on Coupons after 15 Days

	C	O	Na	Si	S	Cl	Fe
control	22.50	15.50	4.35	6.36	2.33	1.16	47.81
SRB	25.82	13.33	2.89	7.64	6.42	0.80	43.09

Figure 3 shows the contact angle image of carbon steel after 15 days of immersion in the control and SRB system. The contact angle of carbon steel for the control system and SRB system was 71.4 and 65°, respectively. The decrease in the surface hydrophobicity of carbon steel under the SRB system can be attributed to the fact that EPS contains more hydrophilic functional groups such as hydroxyl, phosphate, and carboxylic groups.[29]

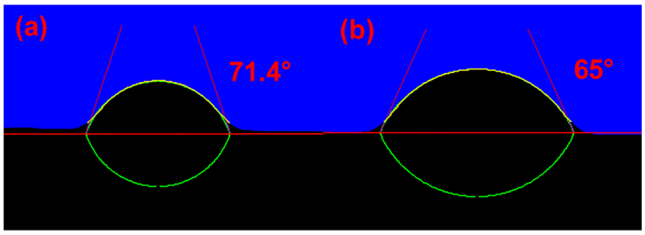

Figure 3. Contact angle photos of carbon steel immersed in corrosion solution for 15 days: (a) control and (b) SRB.

2.3. Corrosion Morphology after Removing Corrosion Products. Figure 4 shows the SEM images of corrosion products removed from 20# steel samples after 15-day immersion. In the control medium, the carbon steel substrate and scratches during grinding can be seen (Figure 4a). The corrosion cracks are rather small on the surface of carbon steel, which indicates that the corrosion degree is very weak in the control medium (Figure 4b). In the SRB medium, the degree of corrosion is similar to that in the control medium. Nevertheless, large corrosion pits appeared on the surface, which means severe local corrosion promoted by SRB occurs on the surface of the coupon.

The surface profile of the coupon after removal of corrosion products is shown in Figure 4. The color intensity bar indicates the depth of the corrosion pit. In the control medium, the surface of carbon steel is dominated by uniform corrosion (Figure 4c), with only small and sporadic corrosion holes, for which the deepest corrosion pit is 1 μm ($4c_1$). In the SRB medium, the maximum corrosion pit depth on the carbon steel surface increased distinctly to 23.7 μm ($4d_1$). SRB promotes the formation of pits on carbon steel surfaces.

2.4. X-ray Photoelectron Spectroscopy (XPS) Analysis. Figure 5 exhibits high-resolution XPS spectra of Fe 2p, O

https://doi.org/10.1021/acsomega.3c00391
ACS Omega 2023, 8, 13955−13966

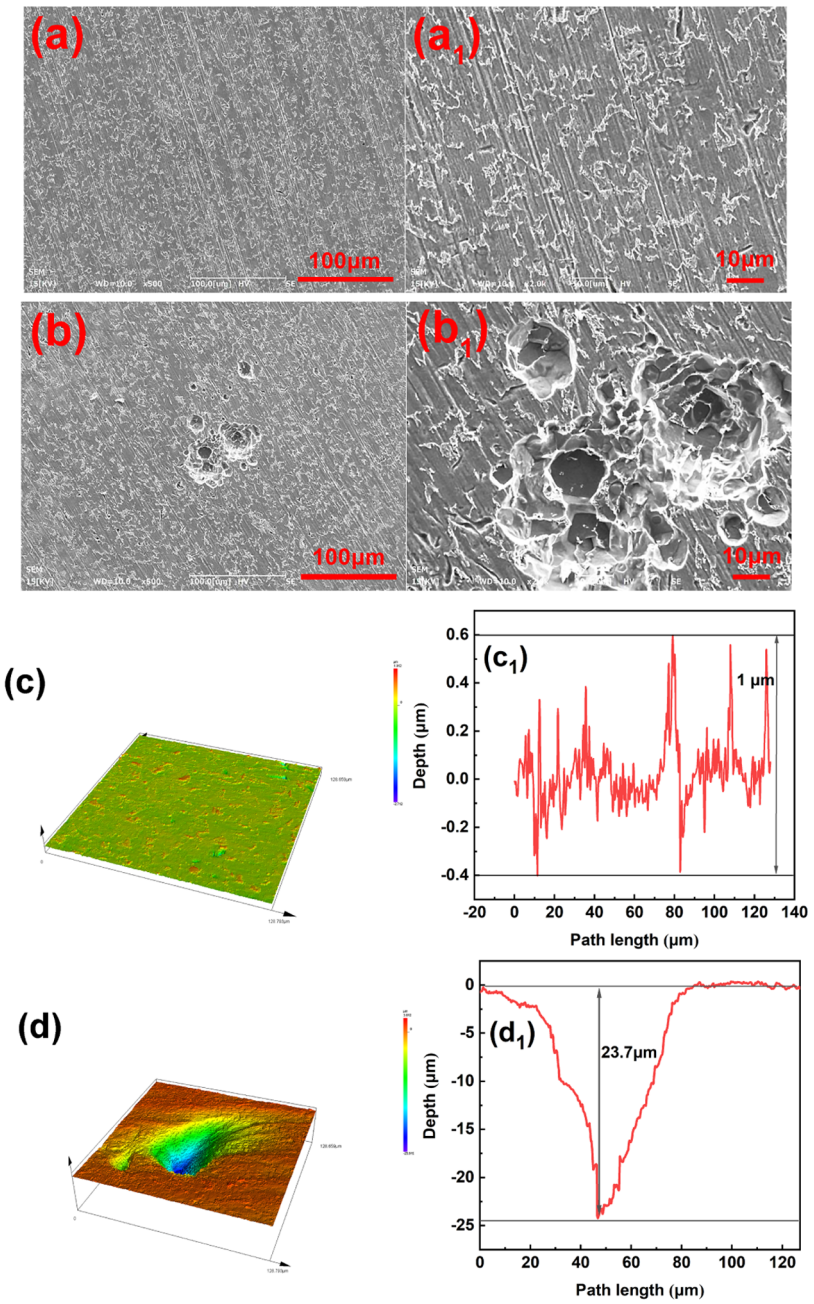

Figure 4. SEM images of the coupon surface (corrosion products removed) after 15-day incubation (a, a_1) in the control medium and (b, b_1) in the SRB medium. Three-dimensional morphology of local corrosion (c, c_1) in the control medium and (d, d_1) in the SRB medium.

1s, C 1s, N 1s, and S 2p of the surfaces of coupons after 15-day incubation with and without SRB. Table 2 shows the reference binding energy. The fitted Fe 2p high-resolution spectra are shown in Figure 5a. The Fe 2p spectrum exhibits five peaks in the control medium. The peaks at 711.4, 713.9, 718.8, 724.5, and 726.4 eV correspond to Fe_2O_3, FeOOH, Fe(II), Fe_2O_3, FeOOH,[30,31] respectively. The Fe 2p spectrum was curve-fitted with five peaks in the SRB medium. The peaks at 710.3 and 724 eV were assigned to FeS,[30,32] which was the typical corrosion product in the SRB medium. The fitted O 1s high-resolution spectra are shown in Figure 5b and the peaks at 529.9, 531.2, and 532.3 eV correspond to Fe_2O_3, FeOOH, and OH^- in the control or SRB medium. The peak of OH^- was attributed to H_2O.[33] The organic O peak at 531.8 eV was attributed to EPS secreted by SRB.[34] The fitted C 1s high-resolution spectra are shown in Figure 5c. The C 1s spectra of the control and SRB systems were fitted by the curve of three peaks. The peaks at 284.8, 286.1, 288.1, and 289.1 eV are for C−S/C−H/C−C,[35] C−N, C═O,[30,36] which could be attributed to the adsorption of HPAM and SPS. The fitted N 1p high-resolution spectra are shown in Figure 5d. The N 1p spectra of the control and SRB systems were fitted by the curve of two peaks. The peak at 399.5 eV was attributed to NH_2 in the HPAM,[36] while the other one at 400.5 eV is due to C−N.[30] The fitted S 2p high-resolution spectra are shown in Figure 5e. The peaks at 167.9 and 168.5 eV were for $SO_3^-Na^+$ in the control or SRB medium.[37] The peaks at 169.4 and 169.9 eV were for SO_4^{2-}.[30] The FeS peak at 159.2 eV was the result of the corrosion products formed in the SRB medium. $SO_3^-Na^+$, C−N, and NH exist in both sterile and inoculated

https://doi.org/10.1021/acsomega.3c00391
ACS Omega 2023, 8, 13955−13966

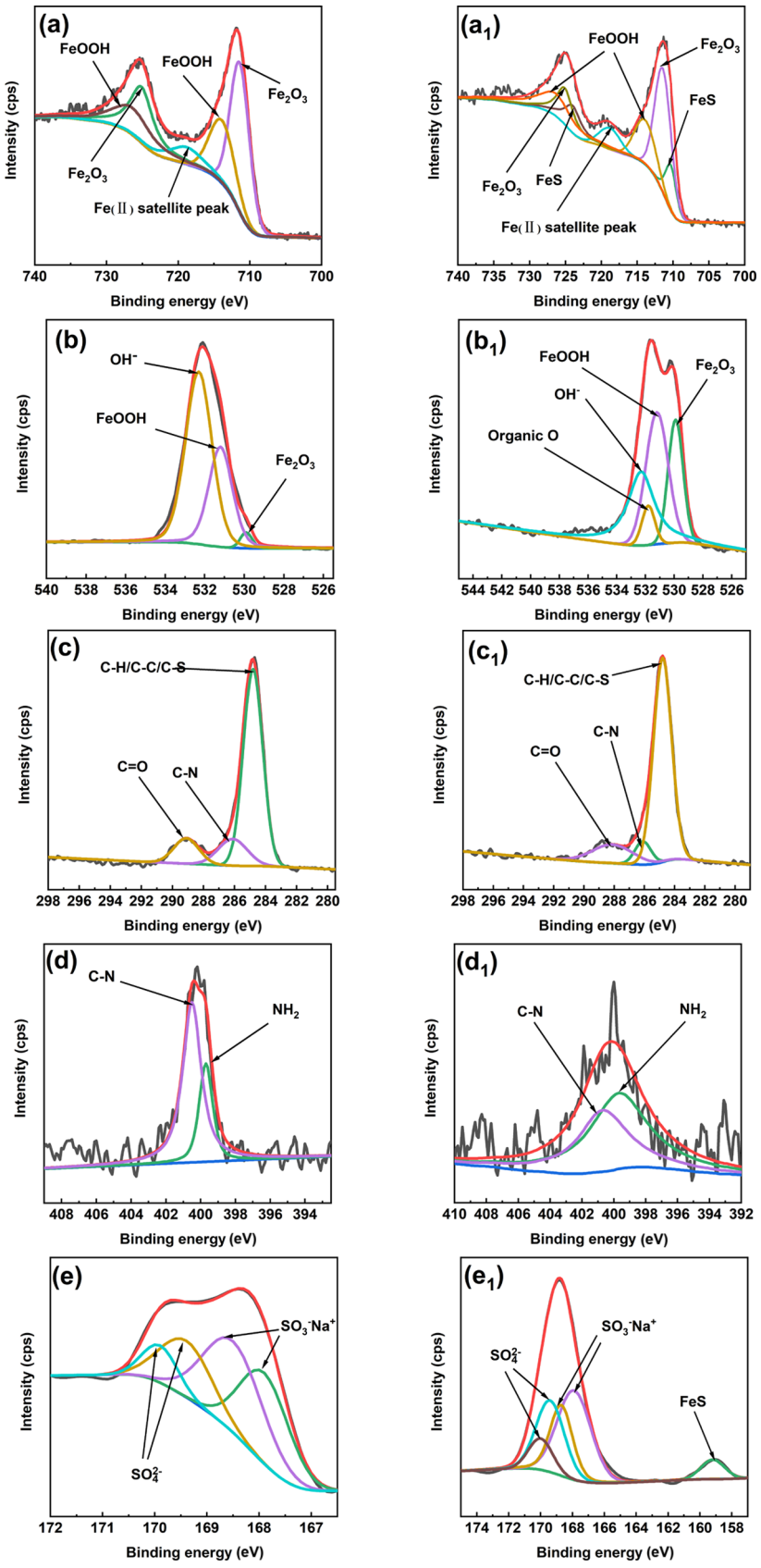

Figure 5. XPS spectra of Fe 2p (a), O 1s (b), C 1s (c), N 1s (d), and S 2p (e) for coupons after 15-day incubation: (a−e) in the control medium and (a_1−e_1) in the SRB medium.

systems, which was caused by the adsorption of HAPM and SPS on the surface of coupons in NaCl ASP flooding. It can be seen from Table 3 that the percentage of N atoms on the surface of carbon steel under the control medium is higher

https://doi.org/10.1021/acsomega.3c00391
ACS Omega 2023, 8, 13955−13966

Table 2. Fitted Parameters for Fe 2p, O 1s, C 1s, N 1s, S 2p Spectra and the Elemental Compositions of the Coupon Surface after 15 Days in the Control and SRB Medium

valence state	sample surface	binding energy (eV)	proposed components	relative quantity
Fe 2p	control	711.4	Fe_2O_3	0.34
		713.9	FeOOH	0.19
		718.8	Fe(II) satellite peak	0.09
		725.1	Fe_2O_3	0.22
		726.4	FeOOH	0.16
	SRB	710.3	FeS	0.08
		711.4	Fe_2O_3	0.31
		713.9	FeOOH	0.14
		718.8	Fe(II) satellite peak	0.07
		724	FeS	0.1
		725.1	Fe_2O_3	0.13
		726.4	FeOOH	0.17
O 1s	control	529.9	Fe_2O_3	0.03
		531.2	FeOOH	0.34
		532.3	OH^-	0.63
	SRB	529.9	Fe_2O_3	0.23
		531.2	FeOOH	0.37
		531.8	organic O	0.06
		532.3	OH^-	0.34
C 1s	control	284.8	C−S/C−H/C−C	0.73
		286.1	C−N	0.15
		289.1	C═O	0.12
	SRB	284.8	C−S/C−H/C−C	0.76
		286.1	C−N	0.08
		288.1	C═O	0.16
N 1p	control	399.7	NH_2	0.29
		400.5	C−N	0.71
	SRB	399.7	NH_2	0.59
		400.5	C−N	0.41
S 2p	control	167.9	$SO_3^+Na^-$	0.32
		168.5	$SO_3^+Na^-$	0.38
		169.4	SO_42^-	0.21
		169.9	SO_42^-	0.09
	SRB	159.2	FeS	0.06
		167.9	$SO_3^+Na^-$	0.37
		168.7	$SO_3^+Na^-$	0.22
		169.4	SO_42^-	0.26
		170.0	SO_42^-	0.09

Table 3. Atomic Percentage for Fe 2p, O 1s, C 1s, N 1s, and S 2p Spectra of the Surface Films on the Coupons after 15-Day Incubation with and without SRB

atom (%)	Fe	C	O	S	N
control	5.24	44.3	41.43	2.78	6.25
SRB	6.6	57.54	26.46	4.69	4.81

than that under the SRB medium, which may be caused by more HPAM adsorption on the surface under sterile conditions. $SO_3^-Na^+$ accounts for 70 and 59% (Table 2) of the peak areas of the S 2p spectrum under sterile and inoculation conditions, respectively, indicating that there is less adsorption of SPS.

2.5. Electrochemical Measurements. In the control medium (Figure 6a), the diameter of the Nyquist plot exhibited an increasing trend 6 days before immersion, which can be attributed to the formation of a protective layer on the carbon steel surface. The Nyquist plot diameter decreases from 6 to 12 days, then gradually increases with time, which indicates that the protective layer is damaged and then formed.[24] It can be seen from Figure 7b$_1$ that there are two-time constants and only one capacitive reactance arc in the control medium. The intensified corrosion reaction will cause the real part of the capacitive arc to shrink in the low-frequency region. Meanwhile, the protection of the carbon steel metal matrix by the product film will lead to the increase of the capacitive arc in the low-frequency region. Consequently, the impedance spectrum of the control medium is characterized by one capacitive reactance arc and two peaks.

In the SRB medium (Figure 6b), the Nyquist plot diameter first decreases, then increases, and finally stabilizes. After 9 days of immersion, bode phase angle vs log frequency plots changed significantly, and a third phase angle peak appeared. In electrochemical impedance spectroscopy, time constant is the embodiment of the Faraday impedance influencing factor. In the early stage of immersion, the two-phase angles were formed due to the influence of corrosion products and adsorption layers on the state variables of the electrode system. At this stage, the state variable of the electrode system is not large enough to be affected by the thin biofilm. With the formation of a gradually perfected biofilm, the state of the film layer on the electrode surface changed after 6 days. The mass transfer process of the reactive particles involved in the interfacial corrosion reaction may also be a slow step. Consequently, a third time constant appears in the Bode phase angle.

The equivalent circuit of two-time constants and three-time constants are shown in Figure 7. According to the phase angle vs frequency curves in Figure 6b, the control state and 1−4 days of SRB state are fitted by an equivalent circuit with two constants (Figure 7a), and the 6th day of the SRB state is fitted by an equivalent circuit (Figure 7b). The 9−15 days of the SRB state is fitted by an equivalent circuit with three constants (Figure 7c). In the equivalent circuit, R_s represents the solution resistance, R_1 and Q_1 the resistance and the capacitance of the biofilm, R_2 and Q_2 represent the resistance and the capacitance of the corrosion products, R_{ct} and Q_{dl} represent charge transfer resistance and double-layer capacitance, W represents the Warburg diffusive impedance, and n represents the diffusion coefficient. Q is constant phase components, and the impedance Z_Q is expressed as follows: $Z_Q(w) = [Y_0(j\omega)^n]^{-1}$ where Y_0 is the admittance magnitude of the CPE, ω is the angular frequency, and n is the dispersion coefficient. The fitted data are shown in Table 4.

Figure 8 shows charge transfer resistance R_{ct} under different conditions. In the control medium, with the increase of immersion time, the charge transfer resistance R_{ct} increases first, then decreases, and finally tends to be stable. In the SRB medium, R_{ct} first decreased, then increased, and finally tends to be stable. In the first 2 days, R_{ct} of the SRB medium is higher than that of the control medium, which indicates that the corrosion of the electrode in the SRB medium is less severe than that in the control medium. From day 2, R_{ct} of the SRB medium becomes much less than that of the control medium, which indicates that the corrosion of the electrode in the SRB medium grows faster than that in the control medium.

Figure 9 shows the potentiodynamic polarization curves of carbon steel in the control and SRB medium after 15 days. The fitted electrochemical parameters are listed in Table 5. The corrosion potential of carbon steel in the SRB medium shifts toward the negative. Compared to the control medium, SRB

https://doi.org/10.1021/acsomega.3c00391
ACS Omega 2023, 8, 13955−13966

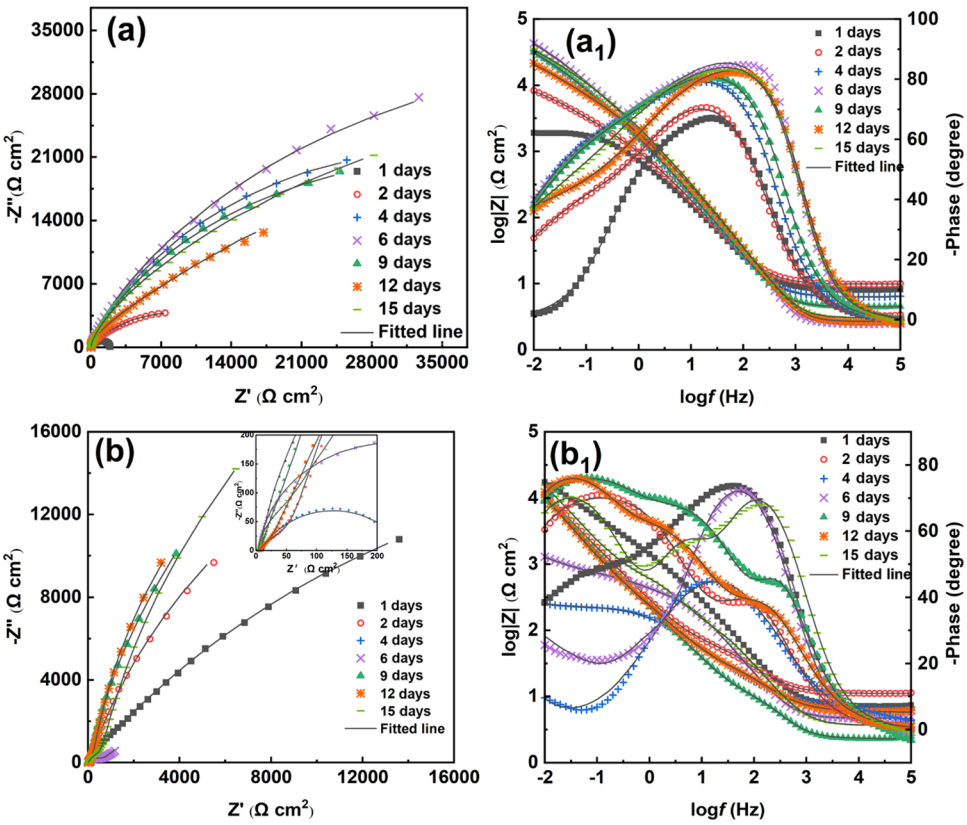

Figure 6. Nyquist and Bode plots of the electrode with time (a, a_1) control medium and (b, b_1) SRB medium.

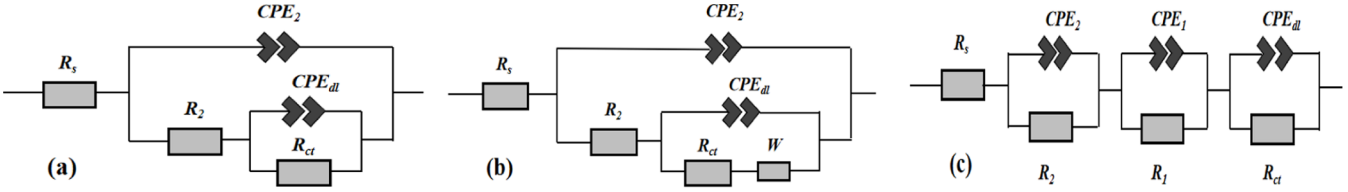

Figure 7. Equivalent circuit of electrochemical impedance spectroscopy (EIS) data fitting: (a) control system and SRB system for 1−4 days; (b) the 6th day of the SRB system; and (c) the SRB system for 9−15 days.

Table 4. EIS Fitting Parameters of Control and SRB Systems

	time (days)	R_s (Ω cm²)	CPE_1 (Ω^{-1} s^n cm^{-2})	R_1 (Ω cm²)	CPE_2 (Ω^{-1} s^n cm^{-2})	R_2 (Ω cm²)	CPE_{dl} (Ω^{-1} s^n cm^{-2})	R_{ct} (Ω cm²)	W (Ω^{-1} s^n $cm^{-0.5}$)
control	1	8.01			1.61×10^{-4}	707.8	2.39×10^{-4}	1.23×10^{3}	
	2	9.87			1.38×10^{-4}	1236	3.45×10^{-4}	7.16×10^{3}	
	4	6.37			8.90×10^{-5}	2095	9.51×10^{-5}	3.13×10^{4}	
	6	2.46			5.15×10^{-5}	1153	8.02×10^{-5}	4.32×10^{4}	
	9	4.50			8.12×10^{-5}	1652	9.60×10^{-5}	2.98×10^{4}	
	12	2.69			4.79×10^{-5}	397.4	1.46×10^{-4}	2.61×10^{4}	
	15	3.09			4.35×10^{-5}	404.1	8.64×10^{-5}	3.71×10^{4}	
SRB	1	7.13			7.15×10^{-5}	1057	2.13×10^{-4}	1.62×10^{4}	
	2	11.04			2.40×10^{-4}	74.95	5.69×10^{-4}	1.11×10^{4}	
	4	6.17			2.46×10^{-4}	240.6	8.29×10^{-4}	2.38×10^{2}	
	6	4.66			1.31×10^{-5}	256.2	6.67×10^{-4}	9.76×10^{2}	4.83×10^{-3}
	9	2.30	3.48×10^{-3}	68.25	2.51×10^{-4}	45.82	1.04×10^{-3}	1.08×10^{4}	
	12	5.82	4.89×10^{-4}	13.76	2.09×10^{-4}	246.2	1.24×10^{-3}	9.94×10^{3}	
	15	3.68	1.25×10^{-4}	50.64	2.87×10^{-4}	446.6	7.02×10^{-4}	1.52×10^{4}	

promotes the anode reaction process while inhibiting the cathode reaction process. The corrosion current in the SRB medium is higher than that in the control medium, indicating that SRB promotes the corrosion of metals.

3. DISCUSSION

3.1. Corrosion Behavior of Pipeline Steel in the Production System of NaCl ASP Flooding. XPS analysis showed that the corrosion products on the surface of coupons

https://doi.org/10.1021/acsomega.3c00391
ACS Omega 2023, 8, 13955−13966

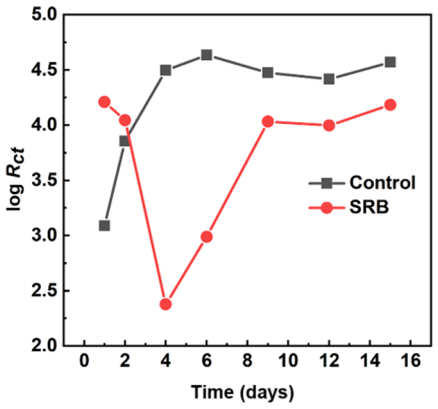

Figure 8. Change of R_{ct} with time in different systems.

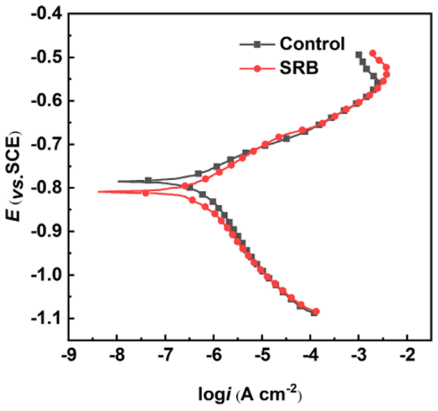

Figure 9. Polarization curves in different states after immersion for 15 days.

Table 5. Fitted Results from Abiotic Potentiodynamic Polarization Curves in Figure 9

	i_{corr} (A cm^{-2})	E_{corr} (V_{vs} SCE)	ba (V dec^{-1})	bc (V dec^{-1})
control	2.479×10^{-7}	−0.78522	0.05267	0.07767
SRB	2.637×10^{-7}	−0.81039	0.06497	0.08904

were Fe_2O_3, FeOOH, and Fe_3O_4. The corrosion process of pipeline steel in the NaCl ASP flooding production system in the control medium was essentially the oxidation of iron and the reduction of oxygen (eqs 1−5)

$$Fe \rightarrow Fe^{2+} + 2e^- \quad (1)$$

$$O_2 + H_2O + 4e^- \rightarrow 4OH^- \quad (2)$$

$$Fe^{2+} + 2OH^- \rightarrow Fe(OH)_2 \quad (3)$$

$$4Fe(OH)_2 + O_2 \rightarrow 4FeOOH + 2H_2O \quad (4)$$

$$2FeOOH \rightarrow Fe_2O_3 + H_2O \quad (5)$$

In the control medium, $SO_3^-Na^+$, C−N, and NH_2 existed on the surface of coupons, which indicated that HPAM and SPS were adsorbed on the surface of carbon steel in NaCl ASP flooding. The research showed the characteristic group of HPAM, amide-$CONH_2$, which forms an adsorption film on the steel surface through the bonding between polar atoms and iron atoms.[38] The HPAM was adsorbed on the metal anode area to provide a network protective film,[39] therefore the contact between the metal and the solution was hindered by electrostatic attraction.[40] The shielding effect of HPAM inhibited the electron loss of Fe atoms in the anode region and inhibited the corrosion of carbon steel. The SPS formed a protective layer on the metal surface to inhibit corrosion through electrostatic attraction.[27] The corrosion of carbon steel was inhibited by HPAM and SPS, and the diffusion of dissolved oxygen in the early stage was inhibited by the high viscosity of the system. Nevertheless, it was observed from the Bode diagram that the phase angles at 1 and 2 days were small, which may be caused by a thinner protective layer due to less HPAM and SPS adsorption. Owing to the thin protective layer in the early stage of immersion, Cl^- penetrated the protective layer and caused corrosion of carbon steel.[41] Consequently, the R_{ct} of the control medium in the early stage was smaller. With the increase in immersion time, $Fe(OH)_2$ was transformed into dense Fe_3O_4, so the corrosion rate of carbon steel decreased. After 15 days of immersion, the relatively dense FeOOH decomposed into Fe_2O_3, which led to attenuation of the corrosion product layer and accelerated corrosion at the same time. Except that the R_{ct} was small in the early stage, R_{ct} maintained at a high level for the rest of the days. It can be seen from the surface morphology that the corrosion degree of the surface of coupons was weak (Figure 4a$_1$).

3.2. Corrosion Behavior of Produced Liquid Pipeline Steel of NaCl ASP Flooding by SRB. No bacterial cells were observed on the surface of the test piece in the sterile control system. Therefore, the only variable under the inoculation system was SRB. The corrosion of pipeline steel was obviously promoted by SRB, and the existence of SRB in the system will make the corrosion reaction more complicated. It can be seen from XPS that FeS existed in the corrosion products. During the MIC process in the presence of SRB, the main anodic and cathodic reactions were the oxidation of iron and the reduction of sulfate, respectively (eqs 6 and 7).

$$SO_4^{2-} + 9H^+ + 8e^- \rightarrow HS^- + 4H_2O \quad (6)$$

$$Fe^{2+} + HS^- \rightarrow FeS + H^+ \quad (7)$$

The local corrosion of carbon steel was significantly increased by SRB (Figure 4d). After 15 days of immersion, the local corrosion pit depth of carbon steel reached 23.7 μm (Figure 4d$_1$). The author's previous work showed that the adsorption of polymers and surfactants has an inhibitory effect on the corrosion of metals,[42] but this study shows that it has no inhibitory effect on localized corrosion caused by SRB. The XPS results showed FeS and organic oxygen, and the EDS results indicated that SRB participated in the reaction of the medium.

Figure 10 shows the corrosion mechanism of 20# carbon steel produced by NaCl ASP flooding in the presence of SRB. In the SRB medium, the trace of DO in the system inhibited the activity of SRB.[14,43] HPAM was consumed by SRB as an organic carbon source for growth, which could reduce the viscosity of the system. However, SRB needed some time to adapt to the environment. Consequently, the number of SRB was small in the initial stage (stage 1). Nevertheless, the formation of the protective biofilm on the metal surface at the initial stage of immersion results in large R_{ct}.[44] In addition, the biofilm formed at this stage can change the properties of the metal substrate surface, thus facilitating the adhesion of microorganisms on the substrate surface.[45]

The corrosion rate of the SRB system was higher than that of the control system except for 1−2 days (Figure 8), which

https://doi.org/10.1021/acsomega.3c00391
ACS Omega 2023, 8, 13955−13966

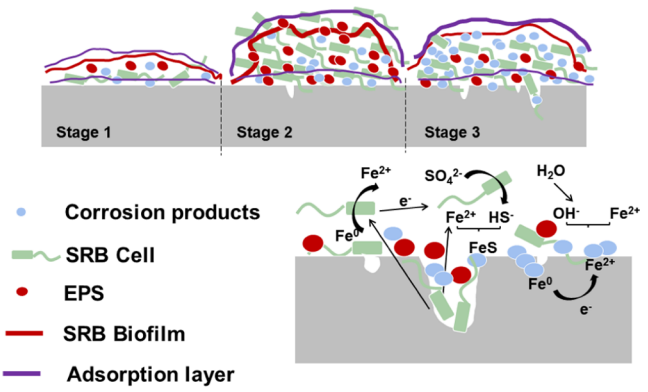

Figure 10. Corrosion mechanism of 20# carbon steel produced by NaCl ASP flooding in the presence of SRB.

can be attributed to the biofilm formed on the surface of the carbon steel. In addition to the nutrients provided by HPAM, the protective layer formed by the adsorption of HPAM and SPS on the surface of carbon steel also had a certain barrier effect on oxygen, which further provided a better environment for SRB on the surface of carbon steel. SRB under anaerobic conditions can reproduce in large numbers, and a large number of metabolites (EPS, corrosion products, and some organic or inorganic substances) on the metal surface are produced through their own metabolic activities.[14,46] Electroactive enzyme molecules in EPS can act as electron carriers to transfer electrons from pipeline steel to O_2,[20] which promoted the cathodic reaction of the electrochemical reaction.[47] The strong complexation of metal cations by EPS could promote the anodic dissolution of the metal.[48] The adsorption of HPAM and SPS on the carbon steel surface was affected by the formation of the biofilm, and SEM images also revealed large differences in the amount of corrosion products in different regions. Hence, after 4 days of immersion, the R_{ct} decreased rapidly, and the corrosion rate of carbon steel increased accordingly.

The diffusion phenomenon was illustrated in the Bode plots (Figure 6b_1) on the 6th day in the SRB medium. At this stage (stage 2), SRB grew exponentially, the biofilm contained a large number of SRB bacteria, metabolites, and corrosion products. The components in the system were converted into insoluble components and deposited on the surface of carbon steel. Under this circumstance, it was difficult for the electrolyte solution and oxygen to pass through the thick biofilm, and the mass transfer process of reactive particles involved in the interfacial corrosion reaction had a slow kinetic process.[49] Some of the corrosion products were stored in the biofilm, where cells had difficulty accessing electron acceptors or obtaining nutrients from external solutions, so they relied on diffusion. Therefore, the *W* impedance was observed on the Nyquist plots (Figure 6b) on the 6th day. The more EPS secreted by the biofilm on the carbon steel surface forms a complex with a large number of ferrous ions,[34,50] and the reaction of the cathode and the anode was promoted by the reduction of Fe^{2+} in the free state. The corrosion of carbon steel was promoted by the weak electrostatic interaction between EPS and metal ions.[51] EPS can promote the formation of corrosion products,[52] and the thicker protective layer had a certain inhibitory effect on corrosion, but the corrosion rate of carbon steel was still high.

After 9 days of immersion (stage 3), three peaks were observed on the Bode plot (Figure 6b_1), which indicated that the metal surface formed a denser biofilm and corrosion products. The promotion of anodic dissolution and the cathodic reaction of carbon steel was weakened by the decreased activity of EPS.[25] It was found that the i_{corr} decreased and R_{ct} increased, while the corrosion rate of carbon steel decreased. After immersion for 15 days, compared with the sterile system, the contact between the carbon steel and the corrosive ions and O_2 in the solution was prevented by the thick protective layer on the surface.[53] The cathodic process of its electrochemical reaction was inhibited (Figure 9). Moreover, the thick protective layer prevented microorganisms from using nutrients in solution to grow, which resulted in iron being directly used by SRB as a nutrient for growth. Meanwhile, the electron transfer process was accelerated by the highly conductive ferrous sulfide. It directly transmits electrons to the specific protein at the sulfate reduction site in the cell, and then the anode dissolved electrons are consumed by sulfate reduction.[19] Consequently, in the later stage of immersion, although the corrosion rate of carbon steel in the SRB medium decreased, it was still higher than that in the control medium.

4. CONCLUSIONS

In this work, the corrosion behavior of 20# carbon steel in the production system of NaCl ASP flooding was investigated by comparing the control and SRB medium. The main conclusions are as follows:

1. The HPAM was used by SRB as a nutrient for growth, resulting in a large loss of viscosity, and the number of SRB is still a large value after 15 days.
2. In the SRB medium, the corrosion of carbon steel at the initial stage of immersion was inhibited by the biofilm formed by SRB on the surface of carbon steel. In the late immersion period, three-time constants appeared in the Nyquist plot of the electrode. The inactivation of EPS resulted in decreased corrosion rates, but still large values.
3. The maximum corrosion pit depth of carbon steel in the SRB medium was 27 times that of the control medium.

5. MATERIALS AND METHODS

5.1. Electrode and Solution. Samples for the corrosion mechanism study were 20# carbon steel with the chemical composition (wt %) of C: 0.17−0.23, Si: 0.17−0.37, Mn: 0.35−0.65, Ni: ≤0.30, Cr: ≤0.15, Cu: ≤0.25, and balance Fe. The samples for the electrochemical test were cut into 1 cm^2 and connected with the copper conductor, with one section exposed and the rest sealed with epoxy resin. The electrode surface was polished using 600, 800, 1000, and 1200-grit silicon carbide paper, then rinsed with acetone and alcohol, and dried in the N_2 gas flow. The samples were used after UV sterilization for 30 min.

The investigated solution was prepared according to the composition of the NaCl ASP flooding system solution from Daqing Oilfield in China. First, simulated water was prepared. It consists of $CaCl_2$ 0.104 g L^{-1}, $MgCl_2$ 0.059 g L^{-1}, Na_2SO_4 0.01 g L^{-1}, Na_2CO_3 3.53 g L^{-1}, and $NaHCO_3$ 0.01 g L^{-1}. A stirrer (IKA MICROSTAR 7.5 C) was used to stir for 2 h at a rotating speed of 400 rpm to prepare 5000 mg L^{-1} polymer mother liquor, which can be used after resting for more than

https://doi.org/10.1021/acsomega.3c00391
ACS Omega 2023, 8, 13955−13966

12 h. The surfactant (sodium petroleum sulfonate) was placed in the polymer mother liquor, then, simulated water and NaCl were added and stirred for 30 min at a speed of 400 rpm to prepare the NaCl ASP flooding simulated solution. In NaCl ASP flooding simulated solution, the polymer content was 600 mg L^{-1}, the salt content was 6600 mg/L, and the surfactant content was 100 mg L^{-1}. The pH of the solution was adjusted to 8. The simulated solution was used after 20 min in an autoclave at 121 °C. The experimental temperature was 35 °C.

5.2. Microbe Cultivation and Inoculation. The SRB was isolated from the production system of NaCl ASP flooding in Daqing Oilfield, China. The SRB culture medium composition was (g L^{-1}): KH_2PO_4 0.5, NH_4Cl 1.0, Na_2SO_4 1.0, $CaCl_2$ 0.05, $MgCl_2{\cdot}6H_2O$ 2.0, $C_6H_8O_6$ 0.1, $C_2H_3NaO_2S$ 0.1, $FeSO_4{\cdot}7H_2O$ 0.5, yeast extract 1.0, sodium lactate 1.1 (pH 7.2).

Each 500 mL culture vial holding 430 mL of artificially produced water was sealed with silicone rubber. The dissolved oxygen concentration in the system solution was measured using a dissolved oxygen analyzer (P6345-01, I-Quip) and it was found to be 3.1 mg L^{-1}. The culture vials were inoculated with 20 mL of SRB exclusive culture medium and 20 mL of seed culture was used as the SRB system. Planktonic SRB (N_{SRB}) was measured by the extinction dilution method.

5.3. Weight Loss and Viscosity Test. After the experiment, the corrosion products on the metal surface were removed by pickling solution (deionized water, HCl, and hexamethylenetetramine). An electronic balance (METTLER TOLEDO MS105) was used to weigh the mass of coupons. The corrosion rate of metal was calculated according to eq 8.

$$V = 8.76 \times 10^4 \times m/s \times t \times d \quad (8)$$

where V is corrosion rate (mm a^{-1}), m is the weight difference before and after corrosion (g), s is the area of coupons immersed in solution (cm^2), t is the corrosion time (h), and d is the metal density (g cm^{-3}).

A viscometer (Brookfield) was used to measure the viscosity of the system at different time nodes.

5.4. Surface Characterization. Prior to the characterization of the surface morphology, the corrosion products were removed by ultrasonic cleaning with pickling solution (hydrochloric acid, hexamethylenetetramine, deionized water), then rinsed with acetone and sterile deionized water, and then dried under a stream of N_2. A laser scanning confocal microscope (LEXT OLS5000) was used to observe the surface morphology of carbon steel after removal of corrosion products. The coupons were soaked in buffer solution containing 2.5% (w/w) glutaraldehyde for 8 h. A scanning electron microscope (SEM) was used to characterize the corrosion products and the specimens with corrosion products were removed. An Optical Contact Angle Meter & Interface Tensiometer (SL200KS) was used to measure the contact angle of the carbon steel surface. XPS (Thermo Scientific EscaLab 250Xi) was used to analyze the composition of corrosion products. A laser confocal microscope was used to observe the surface morphology of carbon steel.

5.5. Electrochemical Measurements. The electrochemical workstation (CS350) was used to perform electrochemical tests. Electrochemical testing was performed using a three-electrode system. 20# steel was used as the working electrode (WE), a saturated calomel electrode was the reference electrode (RE), and a platinum plate was the counter electrode (CE). The test frequency range of EIS is 10^{-2}–10^5 Hz, and the amplitude of the measurement signal is a 10-mV sine wave. EIS data were analyzed using ZSimpWin and an appropriate equivalent circuit model was established. The scanning rate of potentiodynamic polarization curves test was 0.5 mV s^{-1}, and the scanning range was −300 to +300 mV ($_{vs}$OCP).

AUTHOR INFORMATION

Corresponding Author

Qinghe Gao − *Heilongjiang Provincial Key Laboratory of Oilfield Applied Chemistry and Technology, Daqing Normal University, Daqing 163712, China;* orcid.org/0000-0001-7008-8448; Email: gao5510113@163.com

Authors

Li Zhang − *Heilongjiang Provincial Key Laboratory of Oilfield Applied Chemistry and Technology, Daqing Normal University, Daqing 163712, China*

Xin Yu − *Heilongjiang Provincial Key Laboratory of Oilfield Applied Chemistry and Technology, Daqing Normal University, Daqing 163712, China*

He Sun − *Daqing Oilfield Co. Ltd., First Oil Production Plant, Daqing 163001, China*

Yang Ge − *Northeast Petroleum University, Daqing 163318, China*

Chao Wang − *Heilongjiang Provincial Key Laboratory of Oilfield Applied Chemistry and Technology, Daqing Normal University, Daqing 163712, China*

Limin Li − *Heilongjiang Provincial Key Laboratory of Oilfield Applied Chemistry and Technology, Daqing Normal University, Daqing 163712, China*

Jian Kang − *Heilongjiang Provincial Key Laboratory of Oilfield Applied Chemistry and Technology, Daqing Normal University, Daqing 163712, China*

Huijuan Qian − *Heilongjiang Provincial Key Laboratory of Oilfield Applied Chemistry and Technology, Daqing Normal University, Daqing 163712, China;* orcid.org/0000-0002-8817-3963

Complete contact information is available at: https://pubs.acs.org/10.1021/acsomega.3c00391

Notes

The authors declare no competing financial interest.

ACKNOWLEDGMENTS

The authors would like to thank the Natural Science Foundation of Heilongjiang Province (grant no. LH2021B001) and the Daqing Science and Technology Bureau (grant no. zd-2020-19) for the financial support of this project.

REFERENCES

(1) Zhang, G. A.; Yu, N.; Yang, L. Y.; Guo, X. P. Galvanic corrosion behavior of deposit-covered and uncovered carbon steel. *Corros. Sci.* **2014**, *86*, 202−212.

(2) Ding, M.; Yuan, F.; Wang, Y.; Xia, X.; Chen, W.; Liu, D. Oil recovery from a CO_2 injection in heterogeneous reservoirs: The influence of permeability heterogeneity, CO_2 -oil miscibility and injection pattern. *J. Nat. Gas Sci. Eng.* **2017**, *44*, 140−149.

(3) Dong, B.; Xu, Y.; Deng, H.; Luo, F.; Jiang, S. Effects of pipeline corrosion on the injection water quality of low permeability in oilfield. *Desalination* **2013**, *326*, 141−147.

(4) Sheng, J. J. A comprehensive review of alkaline - surfactant - polymer (ASP) flooding. *Asia−Pac. J. Chem. Eng.* **2014**, *9*, 471−489.

(5) Abdel-Wali, A. A. Effect of Simple Polar Compounds and Salinity on Interfacial Tension and Wettability of Rock/Oil/Brine System. *J. King Saud Univ., Eng. Sci.* **1996**, *8*, 153−162.
(6) Jia, R.; Yang, D.; Abd Rahman, H. B.; Gu, T. Laboratory testing of enhanced biocide mitigation of an oilfield biofilm and its microbiologically influenced corrosion of carbon steel in the presence of oilfield chemicals. *Int. Biodeterior. Biodegrad.* **2017**, *125*, 116−124.
(7) Jia, R.; Yang, D.; Abd Rahman, H. B.; Gu, T. An enhanced oil recovery polymer promoted microbial growth and accelerated microbiologically influenced corrosion against carbon steel. *Corros. Sci.* **2018**, *139*, 301−308.
(8) Kokilaramani, S.; Narenkumar, J.; AlSalhi, M. S.; Devanesan, S.; Obulisamy, P. K.; Balagurunathan, R.; Rajasekar, A. Evaluation of crude methanolic mangrove leaves extract for antibiofilm efficacy against biofilm-forming bacteria on a cooling tower wastewater system. *Arabian J. Chem.* **2022**, *15*, No. 103948.
(9) Vigneron, A.; Head, I. M.; Tsesmetzis, N. Damage to offshore production facilities by corrosive microbial biofilms. *Appl. Microbiol. Biotechnol.* **2018**, *102*, 2525−2533.
(10) Kokilaramani, S.; AlSalhi, M. S.; Devanesan, S.; Narenkumar, J.; Rajasekar, A.; Govarthanan, M. Bacillus megaterium-induced biocorrosion on mild steel and the effect of *Artemisia pallens* methanolic extract as a natural corrosion inhibitor. *Arch. Microbiol.* **2020**, *202*, 2311−2321.
(11) AlSalhi, M. S.; Devanesan, S.; Rajasekar, A.; Kokilaramani, S. Characterization of plants and seaweeds based corrosion inhibitors against microbially influenced corrosion in a cooling tower water environment. *Arabian J. Chem.* **2023**, *16*, No. 104513.
(12) Song, X.; Yang, Y.; Yu, D.; Lan, G.; Wang, Z.; Mou, X. Studies on the impact of fluid flow on the microbial corrosion behavior of product oil pipelines. *J. Pet. Sci. Eng.* **2016**, *146*, 803−812.
(13) Xu, D.; Li, Y.; Gu, T. Mechanistic modeling of biocorrosion caused by biofilms of sulfate reducing bacteria and acid producing bacteria. *Bioelectrochemistry* **2016**, *110*, 52−58.
(14) Liu, H.; Cheng, Y. F. Corrosion of X52 pipeline steel in a simulated soil solution with coexistence of Desulfovibrio desulfuricans and Pseudomonas aeruginosa bacteria. *Corros. Sci.* **2020**, *173*, No. 108753.
(15) Liduino, V. S.; Lutterbach, M. T. S.; Servulo, E. F. C. Biofilm activity on corrosion of API 5L X65 steel weld bead. *Colloids Surf., B* **2018**, *172*, 43−50.
(16) Jia, R.; Yang, D.; Xu, D.; Gu, T. Electron transfer mediators accelerated the microbiologically influence corrosion against carbon steel by nitrate reducing Pseudomonas aeruginosa biofilm. *Bioelectrochemistry* **2017**, *118*, 38−46.
(17) Kokilaramani, S.; Al-Ansari, M. M.; Rajasekar, A.; Al-Khattaf, F. S.; Hussain, A.; Govarthanan, M. Microbial influenced corrosion of processing industry by re-circulating waste water and its control measures - A review. *Chemosphere* **2021**, *265*, No. 129075.
(18) Kokilaramani, S.; Rajasekar, A.; AlSalhi, M. S.; Devanesan, S. Characterization of methanolic extract of seaweeds as environmentally benign corrosion inhibitors for mild steel corrosion in sodium chloride environment. *J. Mol. Liq.* **2021**, *340*, No. 117011.
(19) Liu, H.; Cheng, Y. F. Mechanistic aspects of microbially influenced corrosion of X52 pipeline steel in a thin layer of soil solution containing sulphate-reducing bacteria under various gassing conditions. *Corros. Sci.* **2018**, *133*, 178−189.
(20) Beech, I. B.; Sunner, J. Biocorrosion: towards understanding interactions between biofilms and metals. *Curr. Opin. Biotechnol.* **2004**, *15*, 181−186.
(21) Li, D.-p.; Zhang, L.; Yang, J.-w.; Lu, M.-x.; Ding, J.-h.; Liu, M.-l. Effect of H_2S concentration on the corrosion behavior of pipeline steel under the coexistence of H_2S and CO_2. *Int. J. Miner., Metall. Mater.* **2014**, *21*, 388−394.
(22) Biezma, M. V. The role of hydrogen in microbiologically influenced corrosion and stress corrosion cracking. *Int. J. Hydrogen Energy* **2001**, *26*, 515−520.
(23) Fan, M. M.; Liu, H. F.; Dong, Z. H. Microbiologically influenced corrosion of X60 carbon steel in CO_2-saturated oilfield flooding water. *Mater. Corros.* **2013**, *64*, 242−246.
(24) Liu, H.; Fu, C.; Gu, T.; Zhang, G.; Lv, Y.; Wang, H.; Liu, H. Corrosion behavior of carbon steel in the presence of sulfate reducing bacteria and iron oxidizing bacteria cultured in oilfield produced water. *Corros. Sci.* **2015**, *100*, 484−495.
(25) Liu, H.; Gu, T.; Zhang, G.; Liu, H.; Cheng, Y. F. Corrosion of X80 pipeline steel under sulfate-reducing bacterium biofilms in simulated CO_2-saturated oilfield produced water with carbon source starvation. *Corros. Sci.* **2018**, *136*, 47−59.
(26) Han, D.; Jiang, Y. M.; Shi, C.; Deng, B.; Li, J. Effect of temperature, chloride ion and pH on the crevice corrosion behavior of SAF 2205 duplex stainless steel in chloride solutions. *J. Mater. Sci.* **2012**, *47*, 1018−1025.
(27) Jeyaprabha, C.; Sathiyanarayanan, S.; Phani, K. L. N.; Venkatachari, G. Influence of poly(aminoquinone) on corrosion inhibition of iron in acid media. *Appl. Surf. Sci.* **2005**, *252*, 966−975.
(28) Beniken, M.; Driouch, M.; Sfaira, M.; Hammouti, B.; Ebn Touhami, M.; Mohsin, M. A. Anticorrosion Activity of a Polyacrylamide with High Molecular Weight on C-Steel in Acidic Media: Part 1. *J. Bio- Tribo-Corros.* **2018**, *4*, 1−14.
(29) Liang, R.; Li, J.; Liu, M.; Huang, Z. Y. Influence of inhibitors on the adhesion of SRB to the stainless steel in circulating cooling water. *Colloids Surf., B* **2018**, *172*, 1−9.
(30) Wang, J.; Hou, B.; Xiang, J.; Chen, X.; Gu, T.; Liu, H. The performance and mechanism of bifunctional biocide sodium pyrithione against sulfate reducing bacteria in X80 carbon steel corrosion. *Corros. Sci.* **2019**, *150*, 296−308.
(31) Zhang, F.; Liu, J.; Yue, H.; Cheng, G.; Xue, X. Enhanced photo-Fenton catalytic activity by spherical FeS_2 nanoparticles and photoelectric property of hybrid FeS_2/rGO. *Vacuum* **2021**, *192*, No. 110433.
(32) Liang, Y.; Bai, P.; Zhou, J.; Wang, T.; Luo, B.; Zheng, S. An efficient precursor to synthesize various FeS_2nanostructures via a simple hydrothermal synthesis method. *CrystEngComm* **2016**, *18*, 6262−6271.
(33) Luo, X.-P.; Fu, S.-Y.; Du, Y.-M.; Guo, J.-Z.; Li, B. Adsorption of methylene blue and malachite green from aqueous solution by sulfonic acid group modified MIL-101. *Microporous Mesoporous Mater.* **2017**, *237*, 268−274.
(34) Liu, H.; Gu, T.; Asif, M.; Zhang, G.; Liu, H. The corrosion behavior and mechanism of carbon steel induced by extracellular polymeric substances of iron-oxidizing bacteria. *Corros. Sci.* **2017**, *114*, 102−111.
(35) Yang, G.; Xie, Z.; Cran, M.; Ng, D.; Easton, C. D.; Ding, M.; Xu, H.; Gray, S. Functionalizing graphene oxide framework membranes with sulfonic acid groups for superior aqueous mixture separation. *J. Mater. Chem. A* **2019**, *7*, 19682−19690.
(36) Zhi, F.; Jiang, L.; Jin, M.; Xu, P.; Xiao, B.; Jiang, Q.; Chen, L.; Gu, Y. Inhibition effect and mechanism of polyacrylamide for steel corrosion in simulated concrete pore solution. *Constr. Build. Mater.* **2020**, *259*, No. 120425.
(37) Carlini, L.; Fasolato, C.; Postorino, P.; Fratoddi, I.; Venditti, I.; Testa, G.; Battocchio, C. Comparison between silver and gold nanoparticles stabilized with negatively charged hydrophilic thiols: SR-XPS and SERS as probes for structural differences and similarities. *Colloids Surf., A* **2017**, *532*, 183−188.
(38) Amin, M. A.; Ei-Rehim, S. S. A.; El-Sherbini, E. E. F.; Hazzazi, O. A.; Abbas, M. N. Polyacrylic acid as a corrosion inhibitor for aluminium in weakly alkaline solutions. Part I: Weight loss, polarization, impedance EFM and EDX studies. *Corros. Sci.* **2009**, *51*, 658−667.
(39) Banerjee, S.; Srivastava, V.; Singh, M. M. Chemically modified natural polysaccharide as green corrosion inhibitor for mild steel in acidic medium. *Corros. Sci.* **2012**, *59*, 35−41.
(40) Umoren, S. A.; Li, Y.; Wang, F. H. Synergistic effect of iodide ion and polyacrylic acid on corrosion inhibition of iron in H_2SO_4

https://doi.org/10.1021/acsomega.3c00391
ACS Omega 2023, 8, 13955−13966

investigated by electrochemical techniques. *Corros. Sci.* **2010**, *52*, 2422−2429.
(41) Gao, M.; Wang, H.; Song, Y.; Han, E.-H. Corrosion behavior on carbon steel in a simulated soil solution under the interaction effect of chloride and bicarbonate ions. *J. Mater. Res. Technol.* **2022**, *21*, 3014−3024.
(42) Gao, Q.; Yu, X.; Wang, C.; Ge, Y.; Zhang, L.; Li, L.; Kang, J.; Qian, H.; Hou, Z. Effect of oil displacement agent on corrosion behavior of NaCl - Alkali/ Surfactant/ Polymer flooding pipeline steel. *Vacuum* **2023**, *209*, No. 111742.
(43) Wan, Y.; Zhang, D.; Liu, H.; Li, Y.; Hou, B. Influence of sulphate-reducing bacteria on environmental parameters and marine corrosion behavior of Q235 steel in aerobic conditions. *Electrochim. Acta* **2010**, *55*, 1528−1534.
(44) Javed, M. A.; Stoddart, P. R.; Wade, S. A. Corrosion of carbon steel by sulphate reducing bacteria: Initial attachment and the role of ferrous ions. *Corros. Sci.* **2015**, *93*, 48−57.
(45) Enning, D.; Garrelfs, J. Corrosion of iron by sulfate-reducing bacteria: new views of an old problem. *Appl. Environ. Microbiol.* **2014**, *80*, 1226−1236.
(46) Makama, Z.; Celikkol, S.; Ogawa, A.; Gaylarde, C.; Beech, I. The issue with using DNA profiling as a sole method for investigating the role of marine biofilms in corrosion of metallic materials. *Int. Biodeterior. Biodegrad.* **2018**, *135*, 33−38.
(47) Wang, J.; Li, Q.; Li, M. M.; Chen, T. H.; Zhou, Y. F.; Yue, Z. B. Competitive adsorption of heavy metal by extracellular polymeric substances (EPS) extracted from sulfate reducing bacteria. *Bioresour. Technol.* **2014**, *163*, 374−376.
(48) Kobisy, A. S.; Nassar, H. N.; Tawfik, S. M.; Elshatoury, E. H.; Aiad, I. Mitigation of eco-unfriendly and costly microbial induced corrosion using novel synthesized Schiff base cationic surfactants. *J. Chem. Technol. Biotechnol.* **2021**, *96*, 941−952.
(49) Yin, K.; Liu, H.; Cheng, Y. F. Microbiologically influenced corrosion of X52 pipeline steel in thin layers of solution containing sulfate-reducing bacteria trapped under disbonded coating. *Corros. Sci.* **2018**, *145*, 271−282.
(50) Miot, J.; Benzerara, K.; Obst, M.; Kappler, A.; Hegler, F.; Schadler, S.; Bouchez, C.; Guyot, F.; Morin, G. Extracellular iron biomineralization by photoautotrophic iron-oxidizing bacteria. *Appl. Environ. Microbiol.* **2009**, *75*, 5586−5591.
(51) Xie, F. Synergistic Effect between Chloride and Sulfate Reducing Bacteria in Corrosion Inhibition of X100 Pipeline Steel in Marine Environment. *Int. J. Electrochem. Sci.* **2019**, *14*, 2693−2704.
(52) Bao, Q.; Zhang, D.; Lv, D.; Wang, P. Effects of two main metabolites of sulphate-reducing bacteria on the corrosion of Q235 steels in 3.5wt.% NaCl media. *Corros. Sci.* **2012**, *65*, 405−413.
(53) Tawfik, S. M.; Kobisy, A. S.; Badr, E. A.; Elged, A. H.; Lee, Y.-I. Surface-active nonionic conjugated zirconium metal−organic frameworks and their applications; Broad spectrum anti-microbial, anti-SRB biofilm, anti-microbial corrosion. *Environ. Technol. Innovation* **2023**, *29*, No. 103001.

https://doi.org/10.1021/acsomega.3c00391
ACS Omega 2023, 8, 13955−13966